# Strong charge fluctuations in the single-electron box: A quantum Monte Carlo analysis

Carlos P. Herrero
*Institut für Theoretische Festkörperphysik, Universität Karlsruhe, D-76128 Karlsruhe, Germany and Instituto de Ciencia de Materiales, C.S.I.C., Cantoblanco, 28049 Madrid, Spain*

Gerd Schön
*Institut für Theoretische Festkörperphysik, Universität Karlsruhe, D-76128 Karlsruhe, Germany*

Andrei D. Zaikin
*Institut für Theoretische Festkörperphysik, Universität Karlsruhe, D-76128 Karlsruhe, Germany and Lebedev Physics Institute, Leninski pr. 53, 117924 Moscow, Russia*

(Received 6 July 1998)

We study strong electron tunneling in the single-electron box, a small metallic island coupled to an electrode by a tunnel junction, by means of quantum Monte Carlo simulations. We obtain results, at arbitrary tunneling strength, for the free energy of this system and the average charge on the island as a function of an external bias voltage. In much of the parameter range an extrapolation to the ground state is possible. Our results for the effective charging energy for strong tunneling are compared to earlier—in part controversial—theoretical predictions and Monte Carlo simulations. [S0163-1829(99)03108-2]

## I. INTRODUCTION

In the last few years, charging effects in low-capacitance tunnel junctions have been studied extensively, on one hand because of their possible practical applications in single-electron devices, on the other hand because of interesting theoretical questions related to them. These mesoscopic tunnel junctions are generic examples of macroscopic quantum systems with discrete charge states and dissipation.[1–3] They can be fabricated by modern lithographic techniques with junction capacitances as low as $\sim 10^{-15}$–$10^{-16}$ F. In these systems, single-electron tunneling is strongly influenced by the Coulomb interaction at temperatures $T < E_C/k_B \sim 1-10$ K. The simplest device displaying these effects is the so-called single-electron box, where a metallic island is connected via a capacitor $C_G$ and a tunnel junction with capacitance $C_J$ to a gate voltage source $V_G$.[4] This external voltage polarizes the system, which allows a continuous tuning of the properties of the box. The (bare) charging energy of the system is given by a set of parabolas $E(n_G,n)=E_C(n_G-n)^2$ as a function of the *integer* number $n$ of excess electrons in the island and the *continuous* dimensionless gate charge $n_G=C_G V_G/e$. The energy scale and curvature at small $n_G$ is given by $E_C=e^2/2C$. It depends on the capacitance of the island $C=C_G+C_J$, and $e$, the electronic charge. The charging energy is minimized if $n$ is as close to $n_G$ as possible. Hence at low temperatures, $k_B T \ll E_C$, and very weak tunneling in high resistance junctions, $R_t \gg R_K \equiv h/e^2$, $n$ increases in a stepwise fashion as $n_G$ is increased. In the range $-1/2 \leqslant n_G \leqslant 1/2$, which for definiteness we consider in the following, the ground state corresponds to $n=0$, i.e., $E_0(n_G)=E(n_G,0)$. At finite temperatures, higher charge states are excited, and the expectation value $\langle n \rangle_T$ has smeared steps, approaching a linear $n_G$ dependence at high $T$.

In the weak tunneling limit one can proceed perturbatively in an expansion in the dimensionless junction conductance

$$\alpha_t = \frac{1}{4\pi^2}\frac{R_K}{R_t}. \tag{1}$$

In lowest order, transport by sequential single-electron tunneling processes is described by the ''orthodox theory.''[5] On the other hand, the perturbation theory also shows that equilibrium properties, such as the ground-state energy $E_0(n_G)$ and the low-temperature expectation value of the charge $\langle n \rangle = n_G - 1/(2E_C) dE_0(n_G)/dn_G$ get renormalized by electron tunneling processes. The latter is observable as a weakening of the Coulomb blockade.[6,7] In first order in $\alpha_t$ one finds for the two quantities[1,8–11]

$$E_C^* \equiv \frac{1}{2}\frac{d^2}{dn_G^2} E_0(n_G)\bigg|_{n_G=0} = E_C[1-4\alpha_t + O(\alpha_t^2)] \tag{2}$$

and (for $-1/2 < n_G < 1/2$)

$$\langle n \rangle = \alpha_t \ln\left(\frac{1+2n_G}{1-2n_G}\right). \tag{3}$$

We observe that even for weak $\alpha_t$ the corrections are most pronounced near the degeneracy points $n_G = \pm 1/2$. In fact, at the degeneracy points and low temperatures any order perturbation theory fails.

In order to cover stronger tunneling and/or a closer vicinity of the degeneracy points various theoretical approaches have been pursued. Systematic higher order expansions in $\alpha_t$ have been performed for equilibrium,[12,13] as well as transport properties.[14] These expansions describe the system well for weak to intermediate tunneling strength as long as the degeneracy points are avoided or the temperature is not too low. Renormalization-group (RG) techniques[10,15] as well as a par-

 

tial summation of arbitrary order processes, accounting for resonant tunneling phenomena,[16] cover the regime of stronger tunneling. However, these RG approaches have concentrated on two adjacent charge states and require specifying a high-frequency cutoff of the order of the charging energy, thus, introducing an uncertainty, which prohibits a quantitative comparison. This limitation has been overcome in the recent work of König and Schoeller[17] within a ''real-time RG'' approach. By including higher charge states they obtain cutoff-independent results. Concentrating on the renormalization of the density matrix they can further cover nonequilibrium and transport properties. A cutoff-independent expression for $E_0(n_G)$ had also been obtained within a ''noncrossing'' approximation scheme.[11]

When $R_t$ is lower, closer to $R_K$, the electron tunneling leads to strong fluctuations of the charge on the island for all values of $n_G$. In the limit of high tunneling conductances, $1/\alpha_t$ can be treated as a small parameter and nonperturbative effects emerge. Also in this regime a RG analysis has been formulated.[8] Instanton techniques have been developed for the equilibrium properties,[18,19] as well as a real-time saddle point expansion for transport properties.[20] All these approaches[19–23] arrive at the conclusion that in the strong tunneling regime the charging energy $E_C^*$ is renormalized as

$$E_C^* = f(\alpha_t) E_C \exp(-2\pi^2 \alpha_t). \tag{4}$$

While there exists general consensus about the exponential dependence of $E_C^*$ on $\alpha_t$, much controversy remains about the pre-exponential factor. The instanton analysis of Ref. 19 yields $f(\alpha_t) \propto \alpha_t$ for $E_C^* < k_B T \ll E_C$ (which is confirmed by the quasiclassical approach[20]) and $f(\alpha_t) \propto \alpha_t^2$ in the limit $k_B T \ll E_C^*$. In contrast, in Ref. 22 a cubic dependence $f(\alpha_t) \propto \alpha_t^3$ has been found, while Ref. 23 reports a linear dependence for all temperatures. This controversy is one of the motivations for us to revisit the problem.

The expression (4) demonstrates that values of $\alpha_t \gtrsim 0.1$ already correspond to strong tunneling, resulting in a substantial renormalization. [Accordingly, a dimensionless conductance with different numerical coefficients, more suitable for the strong tunneling regime could be defined. To avoid confusion, we prefer to use the weak-tunneling expansion parameter, as defined in Eq. (1), throughout this paper.] In principle, Coulomb blockade effects survive at $T=0$ for any value of $\alpha_t$. For instance, clear signs of Coulomb blockade have been observed for $\alpha_t \sim 0.84$.[7] But the experimental observation of such effects for even larger $\alpha_t$ requires exponentially low temperatures $k_B T \lesssim E_C^*$, and therefore is hard to achieve. Thus, it is of most practical interest to investigate electron tunneling for values of $\alpha_t$ of order 1 and less. For this purpose, and in order to fill the gap between the limits covered by the analytic approaches, we analyze the problem numerically by Monte Carlo (MC) techniques.

MC results for the renormalized charging energy $E_C^*$ had been obtained before by different groups,[15,23,24] and in the limit of small $\alpha_t$ there is a very good agreement among the recent data[23,24] and those of perturbation theory.[12] However, deviations arise for $\alpha_t \gtrsim 0.2$. They increase with increasing $\alpha_t$ and have a *systematic* character, hard to explain within the error bars. One possible source for the discrepancy for large $\alpha_t \gtrsim 0.4$ could be the fact that the simulations of Ref. 24 were done down to substantially lower temperatures (typically $k_B T \gtrsim 2 \times 10^{-3} E_C$) than those of Ref. 23 ($k_B T \gtrsim 10^{-2} E_C$). But this does not account for the differences at smaller $\alpha_t \lesssim 0.4$ where the temperature $k_B T \sim 10^{-2} E_C$ was found to be sufficient for convergence. The published MC data are also not sufficient to resolve the discrepancy concerning the prefactor in Eq. (4).

Other physical quantities of interest are the ground-state energy of the system $E_0(n_G)$ (i.e., the lowest energy band) and the average charge on the island $\langle n \rangle$ as a function of the gate charge $n_G$ for general values of the tunneling strength $\alpha_t$. These quantities have been studied analytically in the limits of weak[10,11,16] and very strong tunneling,[15,19] at finite (not too low) temperatures,[25,26] as well as by the real-time RG analysis of Ref. 17, which appears to cover a larger parameter range. It is clearly of interest to extend these investigations to intermediate values of $\alpha_t$ and low temperature, and to control the analytic results by numerical means.

This paper is devoted to a detailed MC analysis of the single-electron box in the regimes of weak to strong tunneling $0 \leqslant \alpha_t \lesssim 1$. In Sec. II, we describe the model and the computational method employed in our calculations. The MC results for the renormalized charging energy at low and finite temperatures are presented in Sec. III. In Sec. IV, we present the free energy $F(n_G)$ as a function of the gate voltage, and we show results for the mean charge on the island. A discussion of our results and of their relation to other work is given in Sec. V.

## II. MODEL AND COMPUTATIONAL METHOD

### A. Basic formalism

The grand partition function of the single-electron box can be represented in terms of the path integral[1]

$$Z(n_G, \alpha_t) = \int d\varphi_0 \sum_{m=-\infty}^{\infty} \exp(2\pi i m n_G) \times \int_{\varphi_0}^{\varphi_0 + 2\pi m} \mathcal{D}\varphi \exp(-S[\varphi]). \tag{5}$$

Here the ''phase'' variable $\varphi(\tau)$ is conjugate to the island charge, and $m$ is the ''winding'' number of the compact variable $\varphi$. The effective action $S[\varphi]$ is given by

$$S[\varphi] = \frac{1}{4E_C} \int_0^\beta \left( \frac{d\varphi}{d\tau} \right)^2 d\tau + 2 \int_0^\beta d\tau \int_0^\beta d\tau' \, \alpha(\tau - \tau') \times \sin^2 \left[ \frac{\varphi(\tau) - \varphi(\tau')}{2} \right], \tag{6}$$

where the first and the second terms account for the charging energy and the electron tunneling, respectively. The kernel $\alpha(\tau)$ reads in Fourier representation

$$\alpha(\tau) = -\frac{\pi}{\beta} \alpha_t \sum_n |\omega_n| \exp(i\tau\omega_n), \tag{7}$$

for Matsubara frequencies smaller than the electronic bandwidth $|\omega_n| \ll D$. For $D \gg k_B T$, which will be considered here, the kernel takes the form $\alpha(\tau) = \alpha_t (\pi k_B T)^2 / \sin^2(\pi k_B T \tau)$.

Apart from the bare charging energy scale $E_C$, the dimensionless conductance $\alpha_t$, and the temperature, the model depends on the gate charge $n_G$, which is proportional to the applied gate voltage.

The effective action and partition function can be rewritten in terms of the phase fluctuations $\theta(\tau)=\varphi(\tau)-2\pi m\tau/\beta$, with boundary condition $\theta(0)=\theta(\beta)$, in the form

$$Z=\sum_{m=-\infty}^{\infty}\exp(2\pi i m n_G)I_m(\alpha_t,\beta). \tag{8}$$

The coefficients $I_m(\alpha_t,\beta)=\int\mathcal{D}\theta\exp(-S_m[\theta])$ are to be evaluated with the effective action $S_m[\theta(\tau)]=S[\theta(\tau)+2\pi m\tau/\beta]$. They depend on the winding number $m$, the temperature, and the tunneling conductance, but are independent of the gate charge $n_G$. Thus, from a computational point of view, the problem reduces to calculating the relative values of $I_m(\alpha_t,\beta)$, which can be obtained from the Monte Carlo simulations apart from an overall normalization constant. Since the partition function is even and periodic with respect to $n_G$, $Z(n_G)=Z(-n_G)=Z(n_G+1)$, we can restrict our discussion to the region $0\leqslant n_G\leqslant 0.5$.

For low-tunneling conductance, the island charge is quantized and at zero temperature the average number of excess electrons in the box $\langle n\rangle$ is a staircase function of the external voltage. In general, at finite temperatures and arbitrary tunneling the average charge can be determined from the free energy $F=-k_BT\ln Z$ of the island by

$$\langle n\rangle=n_G-\frac{1}{2E_C}\frac{\partial F}{\partial n_G}. \tag{9}$$

From the gate-voltage dependence of the free energy one can, further, define a temperature-dependent effective charging energy for the single-electron box as

$$E_C^*(T)=\frac{1}{2}\left.\frac{\partial^2 F}{\partial n_G^2}\right|_{n_G=0}=E_C\left(1-\left.\frac{\partial\langle n\rangle}{\partial n_G}\right|_{n_G=0}\right). \tag{10}$$

The zero-temperature limit of this quantity $E_C^*\equiv E_C^*(0)$ is the renormalized charging energy discussed in the introduction. It coincides with the classical energy scale $E_C$ for weak tunneling ($\alpha_t\ll 1$), but is renormalized in systems with stronger tunneling conductance. At high temperatures, the free energy $F(n_G)$ depends weakly on $n_G$, and the curvature $E_C^*(T)$ approaches zero. By using Eqs. (8) and (10), this effective charging energy $E_C^*(T)$ can also be expressed as

$$E_C^*(T)=2\pi^2 k_BT\langle m^2\rangle_{n_G=0}, \tag{11}$$

where $\langle m^2\rangle_{n_G=0}$ is a moment of the coefficients $I_m(\alpha_t,\beta)$.

### B. Monte Carlo method

MC simulations have been carried out by the standard discretization of the quantum paths into $N$ (Trotter number) imaginary-time slices.[27] In order to keep roughly the same precision in the calculated quantities, as the temperature is reduced, the number of time-slices $N$ has to increase as $1/T$. We have found that a value $N=4\beta E_C$ is sufficient to reach convergence of $I_m$, even for the lowest studied temperatures and for strong tunneling, where convergence has been reported to be slower.[24] Thus, the imaginary-time step employed in the discretization of the paths is $\Delta\tau=\beta/N\sim 1/(4E_C)$. This means that the high-energy cutoff $\omega_c$ associated with this discretization is $\omega_c\sim 2\pi/\Delta\tau\approx 25E_C$. Repeating the calculation for a few data points with higher values of $N$ and high-energy cutoff did not change our results.

The classical Metropolis MC sampling[28] has been used to obtain finite-temperature results, and to extrapolate, where possible, to $T=0$. The partition function has been sampled according to Eq. (8) for temperatures down to $k_BT=E_C/500$. These low temperatures were necessary to determine the zero-temperature effective charging energy for large tunneling conductance (see below). A simulation run proceeds via successive MC steps (MCS). In each MCS, all path-coordinates are updated. At each studied temperature, the maximum distance allowed for random moves was fixed in order to obtain an acceptance ratio of about 50%. For each set of parameters ($\alpha_t$, $T$), we generated $\sim 3\times 10^5$ quantum paths for the calculation of ensemble-averaged values. The starting configuration for the MC runs was taken after system equilibration at the considered temperature. In general, equilibration runs of about $2\times 10^4$ MCS were sufficient, but in some extreme cases, especially for strong tunneling conductance, equilibration runs of about $1\times 10^5$ MCS were necessary.

In some cases, the acceptance ratio for jumps between different winding numbers during a MC run becomes very low, and sampling by direct jumps is inefficient. This happens, in particular at high temperatures ($k_BT>E_C$), where $I_m/I_0$ is very small for $m\neq 0$ and at low temperatures (especially for strong tunneling), where the most relevant phase paths for different winding numbers are very different. In these cases, we have calculated $I_{m'}$ by carrying out simulations for fixed winding number (e.g., $m$), and evaluating in this fixed-$m$ ensemble the average value

$$R_{mm'}=\langle\exp(S_m[\theta]-S_{m'}[\theta])\rangle_m \tag{12}$$

for $m\neq m'$. The average value $R_{mm'}$ so defined coincides with the ratio $I_{m'}/I_m$, since by definition we have

$$\frac{I_{m'}}{I_m}=\frac{\int\mathcal{D}\theta\exp(-S_m[\theta])\exp(S_m[\theta]-S_{m'}[\theta])}{\int\mathcal{D}\theta\exp(-S_m[\theta])}. \tag{13}$$

It is obvious that these average values fulfill the relation $R_{m'm}=1/R_{mm'}$. We have checked that the results of our MC simulations satisfy this consistency relation within the statistical noise. We have also checked for some sets of parameters ($T$, $\alpha_t$) that this method of calculating relative values of $I_m$ gives the same results as the direct Metropolis method, in which the winding number changes during a MC run.

The MC method allows us to calculate the partition function $Z$ as a function of $T$, $\alpha_t$, and $n_G$. There is, however, a limitation on the parameter range that can be studied by this method. As noted in earlier publications,[15,24] due to the term $\exp(2\pi i m n_G)$ in Eq. (8), the ratio $Z(n_G)/Z(0)$ for $n_G\neq 0$ rapidly approaches 0, as the temperature is lowered. Since the MC method provides the coefficients $I_m$ with a limited accuracy, the partition function $Z(n_G)$ can be determined in a reliable way only when the ratio $Z(n_G)/Z(0)$ is larger than

the numerical error in $I_m$. The temperature range where reliable results can be obtained for a given value of $n_G \neq 0$ reaches to lower values as $\alpha_t$ is increased, since the larger is $\alpha_t$, the slower $Z(n_G)/Z(0)$ decreases at low $T$. We found empirically that the lowest temperature for which the whole range $0 \leqslant n_G \leqslant 0.5$ can be studied by the present method with sufficient accuracy, scales roughly as $k_B T_{min} \sim E_C^*(0)/20$. On the other hand, this limitation does not apply for $n_G \approx 0$. Hence, the effective charging energy $E_C^*(T)$ can be evaluated down to much lower temperatures.

## III. EFFECTIVE CHARGING ENERGY

### A. High-temperature regime

At high temperatures ($k_B T \gg E_C$), the partition function of the single-electron box, including the effect of electron tunneling, can be approximated by an expression similar to the classical result[22]

$$Z \simeq \sum_{n=-\infty}^{\infty} \exp[-\beta \tilde{E}_C (n-n_G)^2] = \sum_{m=-\infty}^{\infty} \exp\left[2\pi i m n_G - \frac{\pi^2 m^2}{\beta \tilde{E}_C(T)}\right]. \quad (14)$$

The temperature-dependent parameter $\tilde{E}_C(T)$ takes into account quantum fluctuations. It reduces to the bare charging energy $E_C$ both in the weak tunneling limit and at high temperatures. In the second form we made use of a Poisson resummation to establish the relation to the winding number representation. At sufficiently high temperatures, where only winding numbers $m = 0, \pm 1$ have a non-negligible contribution ($I_m/I_0 \ll I_1/I_0$ for $|m| > 1$), $\tilde{E}_C(T)$ is well defined. In this case Wang and Grabert[22] expressed the result of a semiclassical calculation, where Gaussian fluctuations around the classical paths are allowed, in the form (14). They find

$$\tilde{E}_C(T) = \frac{E_C}{1 + 2\alpha_t \beta E_C}. \quad (15)$$

As the temperature is lowered, $\tilde{E}_C(T)$ decreases as quantum fluctuations become more prominent. At still lower temperatures it is not guaranteed that the partition function can be parametrized in the form (14).

If the partition function is of the form (14) and $\tilde{E}_C(T)$ can be defined, the latter is related to the effective charging energy $E_C^*(T)$, Eq. (10), by

$$E_C^*(T) = \frac{4\pi^2}{\beta} \exp\left[-\frac{\pi^2}{\beta \tilde{E}_C(T)}\right]. \quad (16)$$

This implies that at high temperatures, $E_C^*(T)$ vanishes proportional to $T \exp[-\pi^2/(\beta E_C)]$.

We determined $\tilde{E}_C(T)$ by fitting the coefficients $I_m$ obtained from the MC simulation to a Gaussian profile. At sufficiently high temperatures, where $I_m$ converges quickly as a function of $m$, this is obviously possible. For this range the results are shown in Fig. 1. Our data points (symbols) are compared with the expression (15) (continuous lines) for several values of $\alpha_t$. An increase in the strength of tunneling and quantum fluctuations leads to a decrease of $\tilde{E}_C$. We observe good agreement between MC and analytic results up to $\beta E_C \sim 0.2$, even for the highest junction conductance considered. For larger values of $\beta$ the high-temperature approximation (15) becomes insufficient, dropping below the MC results.

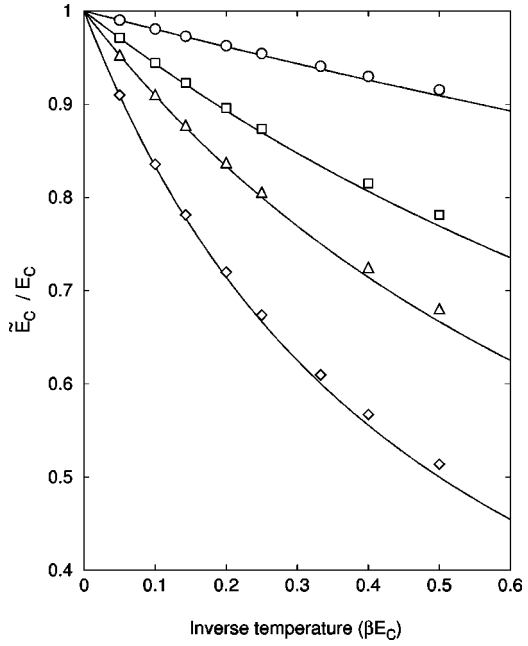


FIG. 1. The parameter $\tilde{E}_C(T)$ is plotted in the high-$T$ region, for several values of the tunneling conductance $\alpha_t$. Symbols indicate results of the Monte Carlo simulations: $\alpha_t = 0.1$ (circles), 0.3 (squares), 0.5 (triangles), and 1 (diamonds). Error bars are smaller than the symbol size. Lines correspond to Eq. (15), derived from semiclassical calculations in Refs. 22 and 29.

In the temperature range shown in Fig. 1, the temperature dependence of the effective charging energy $E_C^*(T)$ is dominated by the exponential term in Eq. (16), i.e., we find vanishingly low values for $E_C^*$, irrespective of the strength of the tunneling conductance.

### B. Low-temperature regime

We now turn to the low-temperature region, where the quantum fluctuations of the island charge dominate the thermal fluctuations and are responsible for the reduction of the effective charging energy $E_C^*(T)$. The latter can be conveniently calculated from the mean-square winding number obtained from MC simulations at finite temperatures, see Eq. (11). Our results are displayed in Fig. 2 for several values of the tunneling conductance $\alpha_t = 0, \ldots, 0.4$. In general, $E_C^*(T)$ grows as the temperature is lowered, and reaches a plateau, the renormalized charging energy $E_C^*(0)$, at low $T$. This saturation of $E_C^*(T)$ should be found for any value of $\alpha_t$. However, for growing $\alpha_t$ lower and lower temperatures are required, consistent with the corresponding decrease of $E_C^*(0)$, which sets the scale for the convergence.

At low temperatures one can also employ an alternative method of calculation of $E_C^*$, and thus provide a consistency check. To do so, we first expand the free energy of the system in powers of $n_G$,

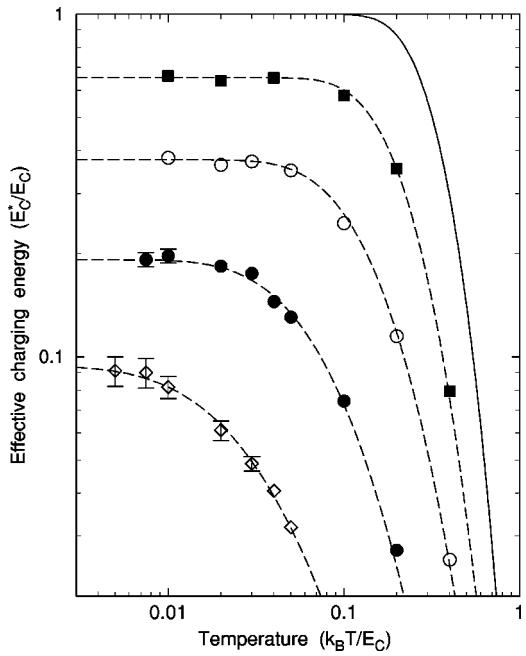


FIG. 2. Effective charging energy $E_C^*(T)$ as a function of temperature for several values of the tunneling conductance. From top to bottom: $\alpha_t=0$ (continuous line), 0.1 (squares), 0.2 (open circles), 0.3 (black circles), and 0.4 (diamonds). Dashed lines are guides to the eye. Error bars are of the order of the symbol size, unless shown explicitly.

$$F(n_G,T)=E_C^*(T)n_G^2+A_4(T)n_G^4+A_6(T)n_G^6+\cdots. \tag{17}$$

Taking a derivative of the partition function in Eq. (8) with respect to $n_G$ we find

$$A_4(T)=\frac{2\pi^4}{3\beta}[3\langle m^2\rangle^2-\langle m^4\rangle]_{n_G=0}, \tag{18}$$

$$A_6(T)=\frac{4\pi^6}{45\beta}[\langle m^6\rangle-15\langle m^4\rangle\langle m^2\rangle+30\langle m^2\rangle^3]_{n_G=0}, \tag{19}$$

and analogous expressions for the higher order terms. Provided that the low-temperature behavior is regular we can conclude from Eq. (11) that for $\beta E_C^*(0)\gg 1$, the average $\langle m^2\rangle$ diverges as $\langle m^2\rangle\propto\beta$. Similarly, one has $\langle m^4\rangle\propto\beta^2$ and $\langle m^6\rangle\propto\beta^3$ in this limit. Since the coefficients $A_n(T)$ are finite at all temperatures including $T=0$, one obtains

$$\langle m^4\rangle/\langle m^2\rangle^2=3+O(1/\beta),\quad \langle m^6\rangle/\langle m^2\rangle^3=15+O(1/\beta), \tag{20}$$

and similar relations for the higher moments of $m$. This implies that at low $T$ the distribution of the coefficients $I_m$ must be close to a Gaussian function of $m$, up to high winding numbers $|m|\lesssim\beta E_C^*(0)$. In other words, in the limit of low $T$ we can rewrite $I_m$ in the form

$$I_m\propto\exp[-a_2(T)m^2-a_4(T)m^4-\cdots], \tag{21}$$

with $a_2(T)\sim 1/(\beta E_C)$ and $a_4(T)\sim 1/(\beta E_C)^2$. Hence, we have $a_4(T)/a_2(T)\sim 1/(\beta E_C)$ [the latter relation can be also derived from the fact that $I_m(T)$ scales at low $T$ as $I_m(T)=I[m/\sqrt{\beta E_C}]$]. Combining Eqs. (8) and (21) and defining $\tilde{E}_C(T)=\pi^2/\beta a_2(T)$ one obtains in the low-temperature limit

$$Z\simeq\sqrt{\frac{\pi}{\beta\tilde{E}_C(T)}}\sum_m \exp[2\pi imn_G-\pi^2m^2/[\beta\tilde{E}_C(T)]]. \tag{22}$$

This relation is valid only for small values of $n_G$, since for $n_G\approx 1/2$ the sum converges slowly and higher values of $m$, for which the $I_m$ are no longer Gaussians, gain importance. Note that this expression for the partition function is formally identical to the high-temperature form given in Eq. (14). An expression similar to Eq. (22) for the low-temperature partition function was given in Ref. 22.

It is easy to show that in the limit $T\to 0$ the two quantities $\tilde{E}_C(0)$ and $E_C^*(0)$ coincide with each other. Indeed, in this limit the sum in Eq. (22) can be replaced by an integral, giving $\langle m^2\rangle_{n_G=0}=\beta\tilde{E}_C(0)/(2\pi^2)$ and the identity $\tilde{E}_C(0)=E_C^*(0)$ becomes obvious. At low but finite $T$ one finds from Eq. (22)

$$\frac{E_C^*(T)}{\tilde{E}_C(T)}\simeq 1-4\beta\tilde{E}_C(T)\exp[-\beta\tilde{E}_C(T)]. \tag{23}$$

The relations described above are well reproduced by our numerical MC analysis. Consistent with the relation (22), at low $T$ the coefficients $I_m$ are well described by a single-Gaussian function, up to high values of $m$, characterized by only *one* parameter $\tilde{E}_C(T)$. This parameter is presented in Fig. 3 as a function of temperature for $\alpha_t=0.5$. Also shown are the results for $E_C^*(T)$. The data points for $\tilde{E}_C(T)$ are indicated by open squares, those for the effective charging energy $E_C^*(T)$ by black circles. Both converge to each other on a temperature scale set by $\tilde{E}_C(T)$, consistent with Eq. (23). We also note that both functions converge to a common plateau at low temperatures, which defines $E_C^*(0)$. Similar convergence is found for all other values of $\alpha_t$; the results for $E_C^*(T)$ and $\tilde{E}_C(T)$ derived from our MC simulations are indistinguishable (within the statistical noise) for temperatures lower than $\sim E_C^*(0)/(5k_B)$.

Clearly, the two methods are not independent from each other. They are equivalent once the Gaussian distribution of the coefficients $I_m$ has been established. However, the fact that at low temperatures the data display the Gaussian distribution with the required accuracy provides a consistency check for our MC procedure. The combination of both approaches increases the reliability by reducing the chance of systematic errors.

For comparison we also present in Fig. 3 the MC results of two different groups for the same tunneling conductance: diamonds[24,29] and open circles.[23] All of them are compatible with those obtained here except for those found in Ref. 24 for $\beta E_C=500$, which lie clearly higher than our general trend.

The results obtained for $E_C^*(0)$ from the low-temperature limit of $E_C^*(T)$ and $\tilde{E}_C(T)$ are shown in Fig. 4 as black symbols. For comparison, we also present analytic and ear-

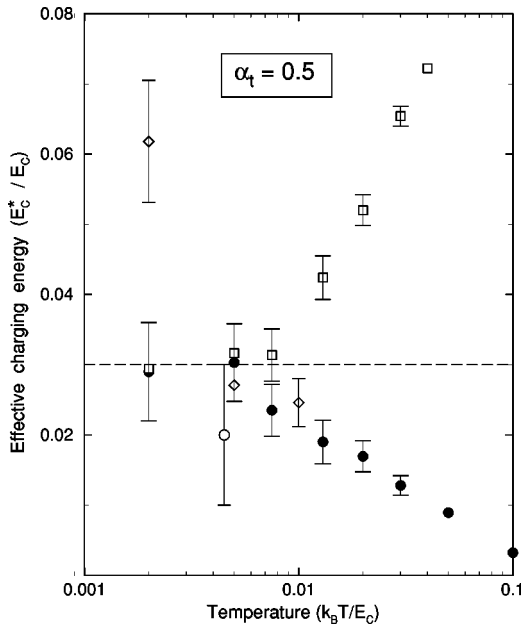


FIG. 3. Convergence of the low-temperature effective charging energy $E_C^*(T)$ as a function of the temperature, for a tunneling conductance $\alpha_t = 0.5$. The results of the present MC simulations are represented by black symbols. Open squares are results for $\tilde{E}_C(T)$ derived from our Monte Carlo simulations. For comparison, results for $E_C^*(T)$ found in earlier MC simulations for the same tunneling conductance are given: Diamonds, data of Wang *et al.* (Ref. 24); open circle, data point of Hofstetter and Zwerger (Ref. 23). Error bars are shown when they are larger than the symbol size. The horizontal-dashed line indicates the value to which our results converge at low temperature.

lier MC results. In Fig. 4(a), we show the data for low to intermediate values of the tunneling conductance $0 \leqslant \alpha_t \leqslant 0.4$ and in part 4(b) we present the effective charging energy $E_C^*(0)$ for the strong-tunneling regime on a semilogarithmic plot. Our MC results (black symbols) follow closely those given by Hofstetter and Zwerger in Ref. 23 (open triangles), while for $\alpha_t > 0.3$ the MC data of Wang *et al.*[24] (open squares) are systematically higher than those found here.

For completeness we add that very recently Göppert *et al.*[13] carried out MC simulations in the charge representation [open circles in Fig. 4(b)], which implies an expansion in $\alpha_t$, rather than the phase representation employed here and in previous MC simulations.[23,24]

In the figure we also present the analytic results of perturbation expansions in the tunneling conductance up to second (dashed-dotted line) and third order (continuous line). In third-order, Göppert *et al.*[13] found for the zero-temperature renormalized charging energy

$$\frac{E_C^*(0)}{E_C} = 1 - 4\alpha_t + A_2\alpha_t^2 + A_3\alpha_t^3 + O(\alpha_t^4), \qquad (24)$$

with $A_2 = 5.066$ and $A_3 = -1.457$. We also show the $\alpha_t$ dependence of the renormalized charging energy $E_C^*(0)$, as obtained from the real-time RG calculations[17] (dashed line). Our numerical values for $E_C^*(0)$ agree with the results of the perturbation expansion and the RG approach for $\alpha_t \lesssim 0.3$.

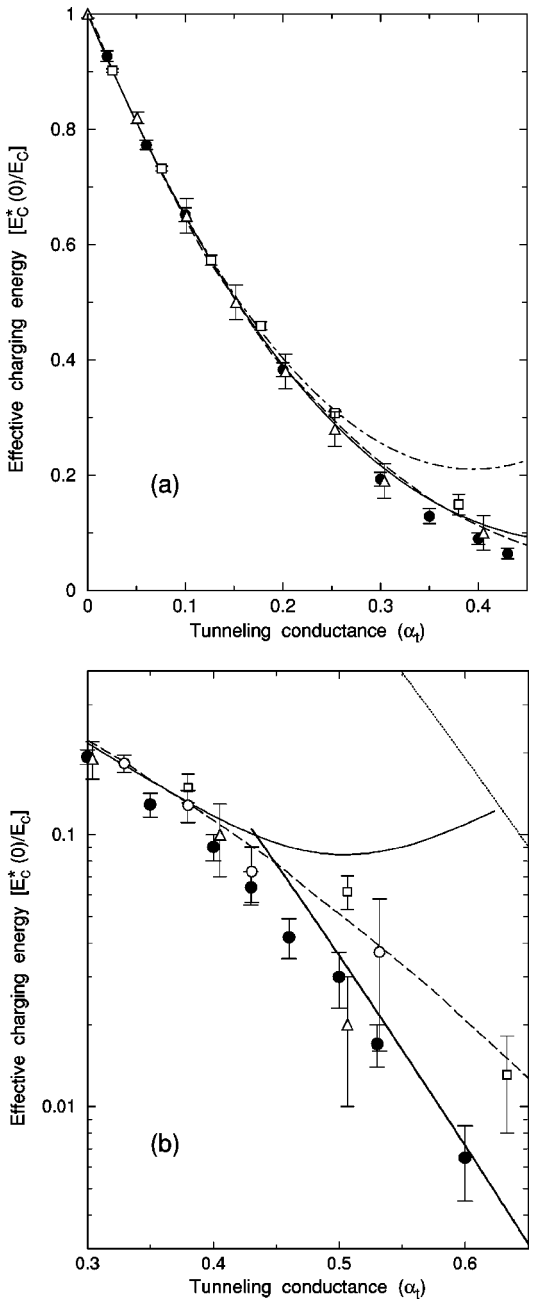


FIG. 4. Low-temperature effective charging energy, $E_C^*(0)$: (a) in the conductance region up to $\alpha_t = 0.4$, and (b) for strong tunneling. Black symbols: results of the present MC simulations. Data from earlier simulations are represented by open symbols: triangles, from Ref. 23, squares from Ref. 24, and circles from Ref. 13. The dashed-dotted and continuous lines correspond to second- and third-order perturbation theory in $\alpha_t$, respectively. The dashed line represents the real-time RG of Ref. 17. The bold and dotted lines in (b) correspond to nonperturbative calculations in Refs. 19 and 22, respectively.

In Fig. 4(b) we display results for $E_C^*(0)$ for stronger tunneling and compare with the predictions of several analytical calculations. In this regime the weak-tunneling expansions fail, while the real-time RG results[17] (dashed line) show a qualitatively correct trend throughout. Already for $\alpha_t \gtrsim 0.5$ our MC results get close (within the error bars) to the result obtained by a nonperturbative instanton calculation[19] (bold line)

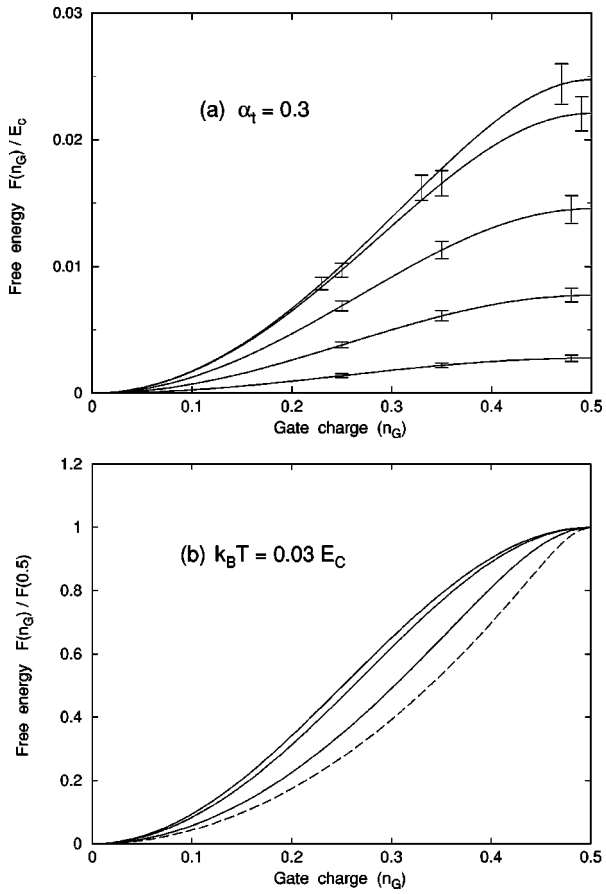


FIG. 5. Free energy vs the dimensionless gate voltage, $n_G$ as obtained from Monte Carlo simulations. (a) Data for junction conductance $\alpha_t=0.3$ and different temperatures. From top to bottom, $k_BT/E_C=$ 0.01, 0.03, 0.05, 0.1, and 0.2. The width of the free-energy band, $F(n_G=0.5)-F(n_G=0)$, decreases as the temperature increases. (b) Same at fixed temperature $k_BT=0.03E_C$, for several values of the tunneling conductance. From top to bottom: $\alpha_t=0.5$, 0.3, 0.1, and 0 (dashed line). For each $\alpha_t$, the free energy has been normalized by its value at $n_G=0.5$.

$$E_C^*(0)=16\pi^4\alpha_t^2 E_C \exp(-2\pi^2\alpha_t+\gamma), \tag{25}$$

where $\gamma$ is Euler's constant. Since the numerics confirms the result (25) already for $\alpha_t\sim 0.5$, and since the accuracy of the instanton analysis[19] should increase with $\alpha_t$, we expect that Eq. (25) remains accurate also in the regime $\alpha_t>0.6$ not covered by our MC simulations. For comparison, we also present in Fig. 4(b) the result for $E_C^*(0)$ found in Ref. 22 for strong tunneling at $T=0$ (dotted line), which predicts a pre-exponential factor $\sim\alpha_t^3$. It lies more than one order of magnitude higher than the results of our MC simulations.

## IV. GATE-CHARGE DEPENDENCE

### A. Free-energy band

The MC method employed here allows us to determine the ''free-energy band'' $F(n_G)$ as a function of the gate voltage $n_G$ at finite temperatures. As an example, we display in Fig. 5(a) results at different temperatures for a dimensionless conductance $\alpha_t=0.3$. The error bars of the Monte Carlo simulations associated with the free energy are largest around $n_G=0.5$. At high temperatures, $F(n_G)$ approaches a cosine shape, $F(n_G)\simeq E_C^*(T)[1-\cos(2\pi n_G)]/(2\pi^2)$, as expected for the classical limit. At low temperatures, the free-energy band is closer to a parabolic shape, which is what we expect in the limit of vanishing junction conductance $\alpha_t\ll 1$, with deviations that are most pronounced near $n_G=1/2$.

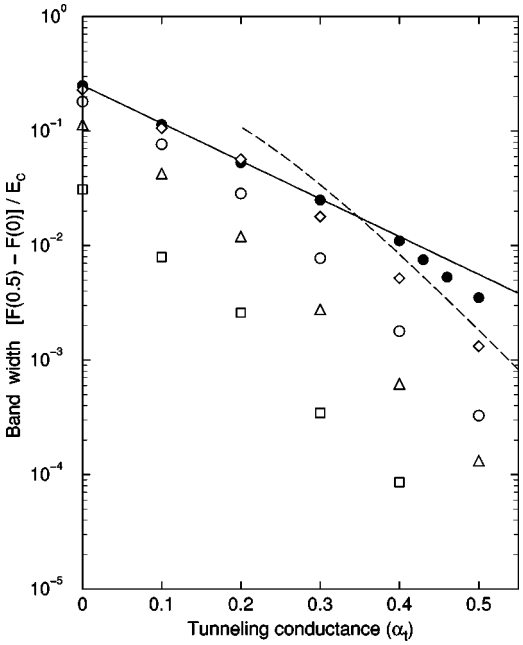


FIG. 6. Width of the free-energy band, $W=F(n_G=0.5)-F(n_G=0)$, as a function of the junction conductance $\alpha_t$ at several temperatures. Open symbols are finite-temperature results for $k_BT/E_C=0.4$ (squares), 0.2 (triangles), 0.1 (circles), and 0.03 (diamonds). Black symbols correspond to the lowest temperature reached in our MC simulations. The continuous line is a fit to the expression $W=W_0\exp(-K\alpha_t)$, with $K=7.6\pm 0.2$. The dashed line is the prediction for the low-temperature bandwidth for strong tunneling (Ref. 19).

A complementary picture is provided in Fig. 5(b). Here $F(n_G)$ is plotted for fixed temperature, $k_BT=0.03E_C$ while $\alpha_t$ is varied. The band is close to a cosine function for large conductance, and clearly differs from this shape for small $\alpha_t$. For the ease of comparison in this figure the free energy has been normalized for each $\alpha_t$ to its value at $n_G=0.5$.

The temperature dependence of the bandwidth $W(T)=F(n_G=0.5)-F(n_G=0)$ is shown in Fig. 6 for several values of $\alpha_t$. For $k_BT>E_C$, one has $W(T)\simeq E_C^*(T)/\pi^2\simeq 4k_BT\exp[-\pi^2/(\beta E_C)]$, as follows from the high-temperature expression for $E_C^*(T)$ given in Eq. (16). In general, one finds that $W(T)$ increases as the temperature decreases, converging to a low-temperature limit. But this convergence is slower than that found for the renormalized charging energy $E_C^*(0)$. The black symbols in Fig. 6 correspond to the lowest temperature we could study for each $\alpha_t$ value. Within the temperature range analyzed here we reached saturation of $W(T)$ only for $\alpha_t\lesssim 0.3$. In this range the low-temperature results can be fitted to an exponential law of the form $W(T=0)=W_0\exp(-K\alpha_t)$ where $W_0=E_C/4$ and $K=7.6\pm 0.2$ (solid line). This is still consistent, within the error bars, with the expression derived for weak tunneling[11] $W=W_0(1-8\alpha_t\ln 2)$. For strong tunneling, one

expects for the bandwidth a similar scaling as a function of $\alpha_t$ as for the renormalized charging energy, i.e., $W(T=0) \sim \exp(-2\pi^2\alpha_t)$. This form, with prefactors as predicted by the instanton calculation of Ref. 19, is shown by the dashed line in Fig. 6. The comparison with our Monte Carlo results reveals differences. While the explicit result of Ref. 19 is not supported, the exponential dependence may be reached at larger values of $\alpha_t$ than covered so far.

Note that even for weak junction conductance [where a good convergence of $W(T)$ to its low-temperature value is demonstrated], the second derivative $F''(n_G)$ close to $n_G = 0.5$ is still changing at the lowest temperatures considered here. This is in line with the results of various analytic calculations,[10–12,16,17] where a logarithmic divergence for $F''(n_G=0.5)$ was found at $T=0$. While this divergence cannot be seen directly in our finite-temperature MC simulations, its precursor is clearly observed: $F''(n_G=0.5)$ increases continuously as temperature decreases for all $\alpha_t$ values considered here.

### B. The charge on the island

The average number of excess electrons in the island $\langle n \rangle$ is of practical interest, since it can be measured directly by measuring the voltage of the box. It follows from the free energy by Eq. (9). In Fig. 7(a) we display $\langle n \rangle$ vs the gate charge $n_G$ at several temperatures for a dimensionless conductance $\alpha_t = 0.1$. As expected, at high temperature the average charge follows closely the line $\langle n \rangle = n_G$, while it decreases for lower $T$ as Coulomb blockade effects become more pronounced. According to the numerical restriction discussed above for the calculation of the partition function $Z(n_G)$, the lowest temperature that could be studied for all values of $n_G$ at $\alpha_t = 0.1$ was $k_B T \sim 0.03 E_C$. For these parameters the average charge $\langle n(n_G) \rangle$ has reached the zero-temperature limit for $0 < n_G \lesssim 0.35$, as can be seen from the convergence of the curves in the figure. For gate charges $n_G$ closer to 0.5, no saturation is found for the temperatures covered, and the $T=0$ value will be lower than our finite-temperature results. Our conclusions are supported by the real-time RG calculations by König and Schoeller.[17] They find a zero temperature $\langle n(n_G) \rangle$ close to our low-temperature results up to $n_G \sim 0.35$. However, consistent with earlier work,[10–12,16] the RG calculations predict at $T=0$ a logarithmic divergence for the slope of $\langle n(n_G) \rangle$ at $n_G = 0.5$. This is beyond the range covered by the MC data. We note, however, that the lowest temperature presented in Fig. 7(a) is not far from the lowest temperatures presently attainable in the laboratory, as for typical values of $E_C/k_B = 1$ K and $T = 20$ mK, one has $k_B T = 0.02 E_C$.

In Fig. 7(b) we present the dependence $\langle n \rangle$ vs $n_G$ for several values of the tunneling conductance, as obtained from MC simulations at a temperature $T = 0.03 E_C/k_B$. In this figure, the tunneling conductance increases from bottom to top, and for the largest $\alpha_t$ shown ($\alpha_t = 0.4$) the dependence is close to a linear one. For comparison, we give also the average charge for the case $\alpha_t = 0$ (dashed line). These finite-temperature results compare well with those found recently from Monte Carlo simulations in the charge representation by Göppert *et al.*[13] at a lower temperature ($\beta E_C = 10^4$). The main difference between our finite-temperature

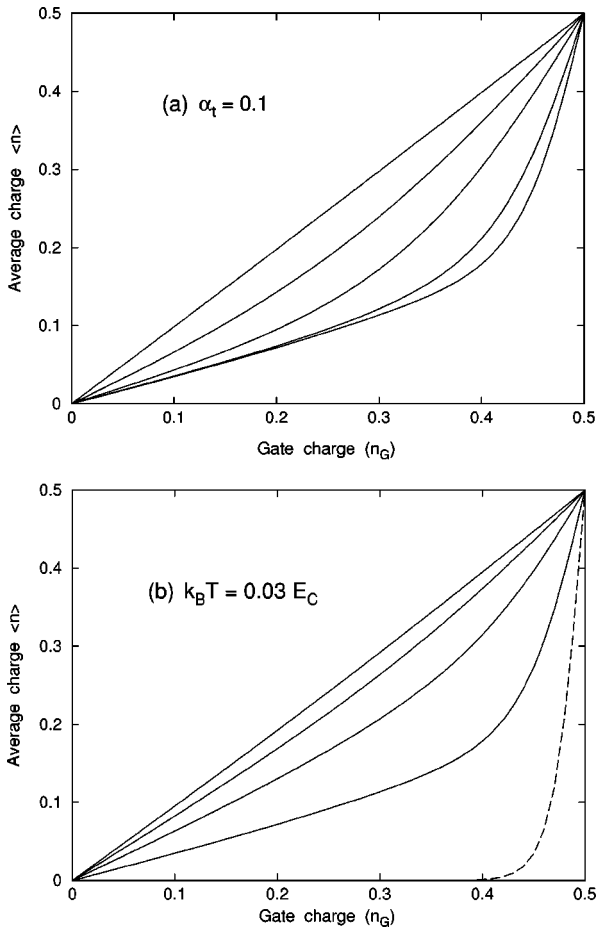


FIG. 7. Average number of excess electrons, $\langle n \rangle$, in the single-electron box. (a) For a dimensionless conductance $\alpha_t = 0.1$ at various temperatures. From top to bottom: $k_B T/E_C = 0.6$, 0.2, 0.1, 0.04, and 0.03. (b) At temperature $T = 0.03 E_C/k_B$ for several values of $\alpha_t$. From top to bottom: $\alpha_t = 0.4$, 0.3, 0.2, and 0.1. For comparison, the average charge for $\alpha_t = 0$ is also given (dashed line).

results and those reported in Ref. 13 is found again in the region close to $n_G = 0.5$, where the above-mentioned logarithmic divergence for $\partial\langle n \rangle/\partial n_G$ is expected to appear.

In order to analyze how long Coulomb blockade effects are observable it is convenient to study the derivative $\partial\langle n \rangle/\partial n_G$ as a function of $n_G$. For $\alpha_t \neq 0$ this derivative has its maximum at $n_G = 0.5$, and it approaches a plateau around $n_G = 0$, the height of which is related to $E_C^*(T)$ by Eq. (10). This decrease is a measure for the strength and observability of charging effects. The results of our MC simulations are presented in Fig. 8 for tunneling conductances in the range $0.1 \leqslant \alpha_t \leqslant 0.5$, at temperature $k_B T = 0.03 E_C$ ($\alpha_t$ decreases from top to bottom). For convenience we normalized $\partial\langle n \rangle/\partial n_G$ by its value at $n_G = 0.5$ for each $\alpha_t$. We see that even for the highest conductance presented, $\alpha_t = 0.5$, charging effects remain observable in the range of temperatures comparable to the corresponding $E_C^*(0)/k_B$: the decrease of $\partial\langle n \rangle/\partial n_G$ at $n_G = 0$ as compared to the value for $n_G = 0.5$ is $\sim 3\%$. A similar conclusion can be reached for other values of $\alpha_t$, i.e., charging effects should be observable (at least) at temperatures of the order of $E_C^*(0)/k_B$ even in the limit of large junction conductances. These results are compatible with recent measurements by Chouvaev *et al.*,[7] where clear

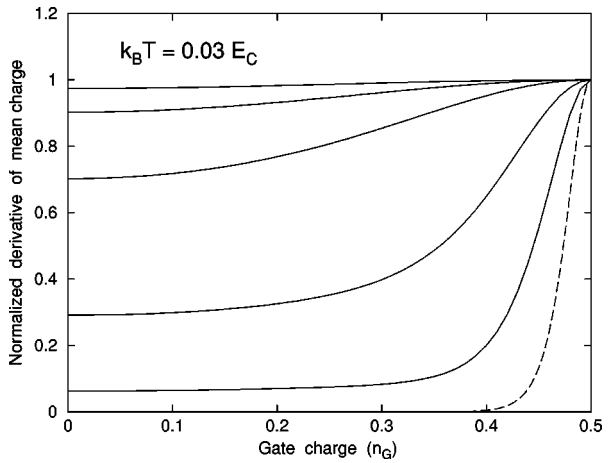


FIG. 8. Derivative of the mean charge in the island with respect to the gate voltage $\partial\langle n\rangle/\partial n_G$ for different values of $\alpha_t$ at $k_BT = 0.03E_C$. From top to bottom: $\alpha_t = 0.5$, 0.4, 0.3, 0.2, 0.1. The dashed line corresponds to the absence of electron tunneling ($\alpha_t = 0$). For each $\alpha_t$, the corresponding curve has been normalized by the value at $n_G = 0.5$.

signs of the persistence of charging effects were observed in a sample with an effective conductance as large as $\alpha_t \approx 0.84$, even at temperatures larger than the renormalized charging energy.

## V. DISCUSSION

The detailed MC analysis carried out in the present paper allows us to determine the low-temperature values of the renormalized charging energy $E_C^*$ for a single-electron box in the range of weak to strong tunneling $0 \leqslant \alpha_t \lesssim 0.6$. Our MC data interpolate well between the perturbative results[12] and those of a nonperturbative instanton analysis[19] in the limits of low and high $\alpha_t$, respectively. Our data demonstrate that the third-order perturbation theory[13] yields quantitatively correct values for $E_C^*$ for $\alpha_t \lesssim 0.3$. On the other hand, we find quantitative deviations at higher values of $\alpha_t$.

A similar conclusion has to be drawn concerning the validity of the RG approach of Ref. 17. This approach is not equivalent to a direct perturbative expansion[12,13] in $\alpha_t$ since it allows for a partial summation of diagrams in all orders in $\alpha_t$. On one hand, for large $\alpha_t$ it works better than the perturbative expansion,[13] capturing the qualitatively correct trend of the renormalized charging energy $E_C^*$ to decrease with increasing $\alpha_t$ up to high values. On the other hand, the neglect of higher-order vertex corrections in the RG may lead to quantitative errors at large $\alpha_t$. While the explicit validity range of the RG analysis is difficult to establish analytically, the corresponding information can be extracted from a comparison to the MC data. This comparison reveals differences between the RG approach[17] and the MC data for $\alpha_t \gtrsim 0.3$.

For stronger tunneling we expect a crossover to an exponential dependence of $E_C^*$ on $\alpha_t$. This is clearly shown by our MC data already at $\alpha_t \gtrsim 0.5$, where it approaches the result of Ref. 19. This crossover is not displayed by the perturbative expansions in powers of $\alpha_t$, and from a general point of view it appears that it cannot be captured within any finite-order expansion. For this reason also MC algorithms formulated in the charge representation may be limited to not too large values of $\alpha_t$. On the other hand, the real-time RG result[17] has been fitted to the exponential dependence (4) for $0.5 \lesssim \alpha_t \lesssim 1$, but it requires a substantially different preexponential function $f(\alpha_t)$ as compared to that found within the instanton approach.[19]

Additional support for both the analytical results obtained in Ref. 19 and our numerical data in the strong tunneling regime comes from an independent MC calculation of Ref. 30. These authors analyzed numerically the correlator $\langle\cos[\varphi(\tau)-\varphi(0)]\rangle$ as a function of temperature at different values of $\alpha_t$, and observed a sharp crossover in the behavior at a temperature $T^*(\alpha_t)$. Since this temperature should be close to the renormalized charging energy $T^*(\alpha_t) \sim E_C^*(0)/k_B$, it is interesting to compare both quantities for different values of $\alpha_t$. This comparison, carried out in Ref. 21, revealed a very good agreement of the data for $T^*(\alpha_t)$ (Ref. 30) with the result of the instanton calculation (25) (see Fig. 1 in Ref. 21), which in turn agrees with our MC data in the strong tunneling regime.

Our numerical data for $E_C^*$ are in agreement with the previous MC data of Ref. 23, extending them to larger $\alpha_t$ and to substantially lower values of the temperature. Although the accuracy of our MC analysis is higher as compared to that achieved in Ref. 23 (the error bars are smaller and the number of points higher), it is satisfactory to observe that our data show the same trend as that found in Ref. 23. Comparing our results to the MC data of Ref. 24 we find good agreement for low $\alpha_t \lesssim 0.3$, while for larger values of $\alpha_t$ their data are *systematically higher*, clearly showing a different trend with increasing $\alpha_t$ as compared to the one indicated by our data. There are several reasons why we believe that this discrepancy cannot be ascribed to insufficiently low temperatures used in our simulation

(i) For all studied values of $\alpha_t \lesssim 0.6$, the calculated $E_C^*(T)$ increases smoothly as the temperature is lowered and it clearly saturates at $k_BT \lesssim E_C^*(0)/5$ (see Fig. 2). The temperature $T = 2\times 10^{-3}E_C/k_B$ is sufficient to observe saturation for all $\alpha_t$ up to $\sim 0.6$. Moreover, a systematic difference between our data and those of Ref. 24 exists already at relatively low-tunneling strengths $0.2 \lesssim \alpha_t \lesssim 0.4$, where the saturation of $E_C^*(T)$ was observed by all groups already at $k_BT \gtrsim 10^{-2}E_C$, i.e., well above the lowest temperature employed in our simulations.

(ii) The quantity $\tilde{E}_C(T)$ converges to *the same* value $E_C^*(0)$, showing saturation at approximately the same temperature $T \lesssim E_C^*(0)/(5k_B)$ as $E_C^*(T)$. This convergence is clearly seen in Fig. 3 for $\alpha_t = 0.5$. The same behavior of $\tilde{E}_C(T)$ was observed for all other values of $\alpha_t$. Since the values $E_C^*(T)$ and $\tilde{E}_C(T)$ were calculated independently, the chance of systematic errors is reduced. Furthermore, these two quantities monotonously converge to the same value from below and from above, respectively, thus providing a lower and an upper bound for $E_C^*(0)$ at each $T$. According to Eq. (23) these bounds should merge at sufficiently low temperatures. This is exactly what our data demonstrate.

(iii) The lowest temperature reached in our MC simulations and in those of Refs. 24 and 29 is the same. We observe

(see, e.g., Fig. 3 for $\alpha_t = 0.5$) that at higher temperatures $k_B T/E_C \sim 0.01$ the data of Wang[29] are still fully consistent both with Ref. 23 and with our data. However, the data point[24,29] at a lower $k_B T/E_C \sim 0.002$ is by more than a factor of 2 higher than all other points. Neither was this result confirmed by our MC analysis, nor do we see any physical reason for such a rapid jump of $E_C^*(T)$ at low $T$, where this quantity should already approach its zero-temperature value.

Very recently one more numerical study of the renormalized charging energy in the strong tunneling regime was performed in Ref. 13, using a different MC algorithm. The data points in Ref. 13 lie in-between our data and those of Ref. 24. Unfortunately, the error bars in Ref. 13 are large for $\alpha_t > 0.4$, thus making a detailed comparison difficult at this stage [see Fig. 4(b)].

In summary, the Monte Carlo method employed here has been shown to be well suited to study charging effects in the presence of an external voltage at not-too-low temperatures. An important advantage of the MC analysis is that it covers both perturbative and nonperturbative regimes and allows us to describe a crossover between them. We conclude that the combination of the expansion (24), the instanton result (25) and the numerical data covers all values of $\alpha_t$, thus providing complete information about the renormalized charging energy $E_C^*$ at low temperatures. The temperature range for which results for the average charge in the island $\langle n \rangle$ can be obtained for $0 \leqslant n_G \leqslant 0.5$, covers most of the temperature region actually studied in the experiments. The Monte Carlo simulations indicate that charging effects are observable in the single-electron box even for strong tunneling, at temperatures of the order of $E_C^*(0)/k_B$.

## ACKNOWLEDGMENTS

We thank G. Falci, F. Guinea, J. König, and H. Schoeller for useful discussions. The work was supported by the Deutsche Forschungsgemeinschaft within SFB 195 and by the INTAS-RFBR Grant No. 95-1305. One of us (C.P.H.) acknowledges financial support from CICYT (Spain) under project No. PB96-0874.

[1] G. Schön and A. D. Zaikin, Phys. Rep. **198**, 237 (1990).
[2] *Single Charge Tunneling*, Vol. 294 of *NATO Advanced Studies Institute, Series B: Physics*, edited by H. Grabert and M. H. Devoret (Plenum, New York, 1992).
[3] *Mesoscopic Electron Transport*, edited by L. L. Sohn, L. P. Kouwenhoven, and G. Schön, Vol. 345 of *NATO Advanced Studies Institute Series E: Applied Sciences* (Kluwer, Dordrecht, 1997).
[4] P. Lafarge, H. Pothier, E. R. Williams, D. Esteve, C. Urbina, and M. H. Devoret, Z. Phys. B **85**, 327 (1991).
[5] D. V. Averin and K. K. Likharev, in *Mesoscopic Phenomena in Solids*, edited by B. L. Altshuler, P. A. Lee, and R. A. Webb (Elsevier, Amsterdam, 1991), p. 173.
[6] P. Joyez, V. Bouchiat, D. Esteve, C. Urbina, and M. Devoret, Phys. Rev. Lett. **79**, 1349 (1997).
[7] D. Chouvaev, L. S. Kuzmin, D. S. Golubev, and A. D. Zaikin, condmat/9803015 (unpublished).
[8] F. Guinea and G. Schön, Europhys. Lett. **1**, 585 (1986); J. Low Temp. Phys. **69**, 219 (1987).
[9] L. I. Glazman and K. A. Matveev, Zh. Eksp. Teor. Fiz. **98**, 1834 (1990) [Sov. Phys. JETP **71**, 1031 (1990)].
[10] K. A. Matveev, Zh. Eksp. Teor. Fiz. **99**, 2598 (1991) [Sov. Phys. JETP **72**, 892 (1991)].
[11] D. S. Golubev and A. D. Zaikin, Phys. Rev. B **50**, 8736 (1994).
[12] H. Grabert, Phys. Rev. B **50**, 17 364 (1994).
[13] G. Göppert, H. Grabert, N. V. Prokof'ev, and B. V. Svistunov, Phys. Rev. Lett. **81**, 2324 (1998).
[14] J. König, H. Schoeller, and G. Schön, Phys. Rev. Lett. **78**, 4482 (1997).
[15] G. Falci, G. Schön, and G. T. Zimanyi, Phys. Rev. Lett. **74**, 3257 (1995); G. Falci, J. Heins, G. Schön, and G. T. Zimanyi, Physica B **203**, 409 (1994).
[16] H. Schoeller and G. Schön, Phys. Rev. B **50**, 18 436 (1994); J. König, H. Schoeller, G. Schön, and R. Fazio, in *Quantum Dynamics of Submicron Structures*, Vol. 291 of *NATO Advanced Studies Institute, Series E: Applied Sciences*, edited by H. A. Cerdeira *et al.* (Kluwer, Dordrecht, 1995); p. 221; H. Schoeller, in *Mesoscopic Electron Transport* (Ref. 3), p. 291.
[17] J. König and H. Schoeller, Phys. Rev. Lett. **81**, 3511 (1998).
[18] A. D. Zaikin and S. V. Panyukov, Zh. Eksp. Teor. Phys. **94**, 172 (1988) [Sov. Phys. JETP **67**, 2487 (1988)]; J. Low Temp. Phys. **73**, 1 (1988).
[19] S. V. Panyukov and A. D. Zaikin, Phys. Rev. Lett. **67**, 3168 (1991).
[20] D. S. Golubev and A. D. Zaikin, Phys. Rev. B **46**, 10 903 (1992), for a related approximation see also A. A. Odintsov, Zh. Eksp. Teor. Fiz. **94**, 312 (1988) [Sov. Phys. JETP **67**, 1265 (1988)].
[21] A. D. Zaikin and S. V. Panyukov, Phys. Lett. A **183**, 115 (1993).
[22] X. Wang and H. Grabert, Phys. Rev. B **53**, 12 621 (1996).
[23] W. Hofstetter and W. Zwerger, Phys. Rev. Lett. **78**, 3737 (1997).
[24] X. Wang, R. Egger, and H. Grabert, Europhys. Lett. **38**, 545 (1997).
[25] D. S. Golubev and A. D. Zaikin, Zh. Eksp. Teor. Fiz. Pis'ma Red. **63**, 953 (1996) [JETP Lett. **63**, 1007 (1996)].
[26] D. S. Golubev, J. König, H. Schoeller, G. Schön, and A. D. Zaikin, Phys. Rev. B **56**, 15 782 (1997).
[27] *Quantum Monte Carlo Methods in Condensed Matter Physics*, edited by M. Suzuki (World Scientific, Singapore, 1993).
[28] K. Binder and D. W. Heermann, *Monte Carlo Simulation in Statistical Physics* (Springer, Berlin, 1988).
[29] X. Wang, Ph.D. thesis, University of Freiburg (Germany), 1996.
[30] R. Brown and E. Simanek, Phys. Rev. B **45**, 6069 (1992).